



# CHORUS

This is the accepted manuscript made available via CHORUS. The article has been published as:

## Pressure-induced large enhancement of Néel temperature and electric polarization in the hexagonal multiferroic $\text{Lu}_{0.5}\text{Sc}_{0.5}\text{FeO}_3$

Fengliang Liu, Changsong Xu, Shoudong Shen, Nana Li, Hangwen Guo, Xujie Lü, Hongjun Xiang, L. Bellaiche, Jun Zhao, Lifeng Yin, Wenge Yang, Wenbin Wang, and Jian Shen

Phys. Rev. B **100**, 214408 — Published 3 December 2019

DOI: [10.1103/PhysRevB.100.214408](https://doi.org/10.1103/PhysRevB.100.214408)

# Pressure-induced large enhancement of Néel temperature and electric polarization in hexagonal multiferroic



Fengliang Liu<sup>1,2\*</sup>, Changsong Xu<sup>3\*</sup>, Shoudong Shen<sup>1\*</sup>, Nana Li<sup>2</sup>, Hangwen Guo<sup>4,5</sup>, Xujie Lü<sup>2</sup>, Hongjun Xiang<sup>1,5</sup>, L. Bellaiche<sup>3</sup>, Jun Zhao<sup>1</sup>, Lifeng Yin<sup>1,4,5</sup>, Wenge Yang<sup>2†</sup>, Wenbin Wang<sup>4,5†</sup> and Jian Shen<sup>1,4,5†</sup>

<sup>1</sup> *State Key Laboratory of Surface Physics and Department of Physics, Fudan University, Shanghai 200433, China*

<sup>2</sup> *Center for High Pressure Science and Technology Advanced Research (HPSTAR), Shanghai 201203, China*

<sup>3</sup> *Physics Department and Institute for Nanoscience and Engineering, University of Arkansas, Fayetteville, Arkansas 72701, USA*

<sup>4</sup> *Institute for Nanoelectronic Devices and Quantum Computing, Fudan University, Shanghai 200433, China*

<sup>5</sup> *Collaborative Innovation Center of Advanced Microstructures, Nanjing 210093, China.*

\*These authors contributed equally.

†Corresponding authors: Wenge Yang (yangwg@hpstar.ac.cn), Wenbin Wang (wangwb@fudan.edu.cn), Jian Shen (shenj5494@fudan.edu.cn)

## Abstract

Hexagonal ferrites ( $h\text{-RFeO}_3$ ) have attracted great attention for their high ferroelectric transition temperature, strong magnetoelectric couplings, and tunable Néel temperature ( $T_N$ ) and electric polarization. While introducing structural distortion has been previously found to be effective to raise  $T_N$  and polarization in  $h\text{-RFeO}_3$ , it is generally difficult to create sizable structural distortion by common approaches including substrate-induced epitaxial strain and chemical doping. Here, we use high-pressure X-ray diffraction measurements to show that pressure can generate large structural distortion and R-layer displacement of  $h\text{-RFeO}_3$ , resulting with dramatic enhancement of polarization and  $T_N$ . Density functional theory calculations reveal that the enlarged  $c/a$  ratio results in a  $\sim 70$  K increase of  $T_N$  along with a significant enhancement of ferroelectric polarization. Our results suggest that pressure is effective to tune structural distortions and related multiferroicity of  $h\text{-RFeO}_3$  system, making  $h\text{-RFeO}_3$  a promising material for spintronic applications.

Recently, multiferroicity of the hexagonal  $RMO_3$  ( $h$ - $RMO_3$  with  $R= Y, Sc$ , rare earth Lu-Dy, and  $M=Fe, Mn$ ) materials has attracted great interest [1-3], especially for hexagonal  $RFeO_3$  ( $h$ - $RFeO_3$ ) that have relatively high magnetic transition temperatures [4-9]. The coexisting spontaneous electric polarization and magnetization, along with the spin reorientation transition, render  $h$ - $RFeO_3$  compounds promising materials for multiferroic applications. In the  $h$ - $RFeO_3$  family,  $LuFeO_3$  has the highest Néel temperature ( $T_N$ ) of 147 K [5-9], which is still too low for room-temperature spintronic applications.

Numerous approaches have been pursued to enhance  $T_N$  [9,10]. In particular, it was proposed that increasing  $c/a$  ratio is an effective way to increase  $T_N$  [10,11]. As a matter of fact, increasing the  $c/a$  ratio in  $h$ - $RMO_3$  system results in a large structural distortion that enhances the super-exchange interaction between transition metal atoms (Fe or Mn), which is beneficial for high magnetic transition temperature [10,11]. For instance, partial substitution of Mn atoms by Fe atoms in  $h$ - $LuMnO_3$  leads to an increase of the  $c/a$  ratio from 1.885 up to 1.925 and yields an increase of  $T_N$  from 100 K to 130 K [10].

Moreover, an enlarged  $c/a$  ratio and structural distortion is closely related to an enhancement of ferroelectric polarization in  $h$ - $RFeO_3$ , which arises from the displacements of R-atom ( $R= Y, Sc$ , rare earth Lu-Dy) layers and tilting in  $FeO_5$  bipyramid [11]. As reported by previous first-principles studies, applying chemical or hydrostatic pressure to hexagonal rare earth ferrites leads to an enhanced “ $K_3$ ” mode distortion, which further results in the increase of the  $c/a$  ratio, as well as enhanced ferroelectric polarization [12]. It is highly desirable to experimentally achieve largest possible  $c/a$  ratio and thus the highest temperature at which multiferroicity can occur in  $h$ - $RMO_3$  materials.

Several methods have been utilized to tune the structure of  $h$ - $RMO_3$  systems. The substrate-induced epitaxial strain has been proven to have limited effects, due to the weak interfacial bonding between substrates and layered  $h$ - $RMO_3$  [9]. Chemical doping appears to be effective in increasing the  $c/a$  ratio of  $h$ - $RMO_3$ , ranging from 1.885 in  $h$ - $LuMnO_3$  up to 1.997 in  $h$ - $Lu_{0.5}Sc_{0.5}FeO_3$  ( $h$ -LSFO) [10]. The highest  $T_N$  in the  $h$ - $RMO_3$  family has been achieved in  $h$ -LSFO which is 172 K [10]. In the present work, we show experimentally that hydrostatic pressure can further dramatically increase the  $T_N$  and ferroelectric polarization in  $h$ -LSFO system. In-situ high-pressure powder x-ray diffraction (XRD) measurements unveil that (i) the hexagonal crystal structure of  $h$ -LSFO is stable up to 35.1 GPa and (ii) The hydrostatic pressure can not only increase the  $c/a$

ratio, but also increases the displacement in R-layer atoms and the tilting angle of the  $\text{FeO}_5$  trigonal bipyramid, which is the main reason for the dramatically enhanced polarization and  $T_N$ . Density functional theory (DFT) calculations show that such distortions yield a large increase in  $T_N$  and ferroelectric polarization [13]. Our study of the pressure effects on  $h$ -LSFO thus provides a powerful solution for tuning structural and physical properties of  $h$ -RMO<sub>3</sub> materials.

## Methods

The hexagonal  $\text{Lu}_{0.5}\text{Sc}_{0.5}\text{FeO}_3$  ( $h$ -LSFO) single crystal was grown using the floating zone technique. First, polycrystalline samples were prepared by a standard solid-state reaction technique.  $\text{Lu}_2\text{O}_3$  was heated at 800°C for 10 hours before use. Stoichiometric ratios of  $\text{Lu}_2\text{O}_3$ ,  $\text{Sc}_2\text{O}_3$  and  $\text{Fe}_2\text{O}_3$  were mixed and thoroughly ground in a mortar. The mixture was pelletized and then sintered at 1350 °C for two days. The resulting powder was packed into latex tubes and pressed into rods of  $\sim 5$ mm in diameter and  $\sim 12$ cm in length under  $\sim 300$  MPa hydrostatic pressure. The obtained rods were sintered at 1380 °C for 10 hours in a vertical furnace. A single crystal of  $\text{Lu}_{0.5}\text{Sc}_{0.5}\text{FeO}_3$  was grown in flowing  $\text{O}_2$  atmosphere at a pressure of 40 bar using a vertical optical image furnace (Model HKZ, SciDre, GmbH, Dresden) equipped with a 3 kW Xenon arc lamp. During growth, the gas flow rate was 0.1 L/min and the upper and lower rods were counter-rotated at 23 and 29 rpm, respectively, to maintain a homogeneous melt. The crystal was grown at a speed of 1mm/h.

Powder lab-based x-ray diffraction (XRD) measurements were performed on the well-crystallized compound on a Bruker D8 Discover diffractometer ( $\lambda = 1.5405 \text{ \AA}$ ) at ambient conditions. Rietveld refinement was conducted on the XRD pattern collected at ambient conditions by using the FULLPROF program [14], which indicates no impurity phases within the accuracy of powder x-ray diffraction measurements. Zero-field-cooled (ZFC) and field-cooled (FC) magnetic susceptibilities of  $h$ -LSFO powder sample as a function of temperature were measured by a Physical Property Measurement System (PPMS, Quantum Design, Inc.) in a magnetic field  $H = 1000$  Oe. Ferroelectric polarization measurement on the single crystal  $h$ -LSFO was performed at room temperature by the TF Analyzer 2000 (aix ACCT Co., Aachen, Germany) using sinusoidal wave current excitations [15].

High-pressure synchrotron powder x-ray Diffraction (XRD) measurements were conducted at room temperature at sector 16BM-D, the Advanced Photon Source (APS), Argonne National Lab (ANL) by using the monochromatic incident X-ray with the wavelength of 0.3263 Å. The powder sample was

first grinded into micrometer size, and then loaded into the sample chamber shaped by rhenium gasket in the Mao-Bell diamond anvil cell [16]. Silicone oil was used as the pressure transmission medium for providing better hydrostatic pressure condition [17], and ruby fluorescence was used to determine the hydrostatic pressure in the sample chamber [18]. The high pressure XRD data were collected with compression range from 0.2 GPa up to 35.1 GPa, and decompression from 35.1 GPa down to 0.1 GPa. The diffraction image was collected by a two-dimensional (2D) X-ray detector (MAR345) at each pressure point. Each diffraction pattern was converted into one dimensional raw data by using the Dioptas software [19]. Rietveld refinement [20] analysis was performed on each pattern to get the structure information by using the GSAS software [21]. The lattice parameters were collected from GSAS refinement.

Density functional theory (DFT) calculations were performed using the Vienna *ab initio* simulation package (VASP) [22]. The generalized gradient approximation (GGA) and the Perdew-Burke Ernzerh of functions for solids [23] were employed. A 500-eV plane wave cutoff energy was used for all calculations along with the projector-augmented wave method [24], with the Lu (5p, 5d and 6s), Sc (3p, 3d and 4s), Fe (3d and 4s), and O (2s and 2p) electrons being treated as valence electrons. A typical effective Hubbard  $U = 4$  eV was also used to treat the localized 3d electrons of Fe ions [25]. Moreover, a  $5 \times 5 \times 3$  k-point mesh was employed for the 30-atom *h*-LSFO cells. The experimental lattice parameters extracted from high pressure XRD measurement at each pressure point are adopted, while the atomic positions are optimized until all Hellman-Feynman forces are smaller than  $0.01$  eV/Å on each ion. Particularly, we worked on a specific (Lu, Sc) configuration that has the displacement patterns of (Lu<sup>up</sup>, Lu<sup>down</sup>, Sc<sup>down</sup>) in one layer and (Lu<sup>up</sup>, Sc<sup>down</sup>, Sc<sup>down</sup>) in the other layer. Such configuration has been proven to have the lowest energy among five considered possibilities in a previous work [25]. Polarizations are calculated using the Berry phase method [26].

## Results

The ambient XRD measurements show that LSFO crystallizes in the  $P6_3cm$  space group (See Section S1 and Fig. S1 in Supplemental Material [27]) as reported before [25,28-29]. Figure 1a shows the diffraction patterns of *h*-LSFO under pressure, evidencing that the crystal structure is robust up to 35.1 GPa (See Section S2 in Supplemental Material [27] for detailed discussion of phase stability of *o*-phase and *h*-phase of  $RFeO_3$ ). Upon increasing pressure, all the Bragg diffraction peaks move

towards higher angles, indicating the shrinkage of lattice constants under pressure (Fig. 1a). Rietveld refinement reveals that each XRD pattern within the pressure range of 35.1 GPa can be well indexed by the original hexagonal structure  $P6_3cm$ , as shown in Fig. 1b, which further demonstrates that the  $YMnO_3$ -type hexagonal structure is preserved under pressure up to 35.1 GPa.

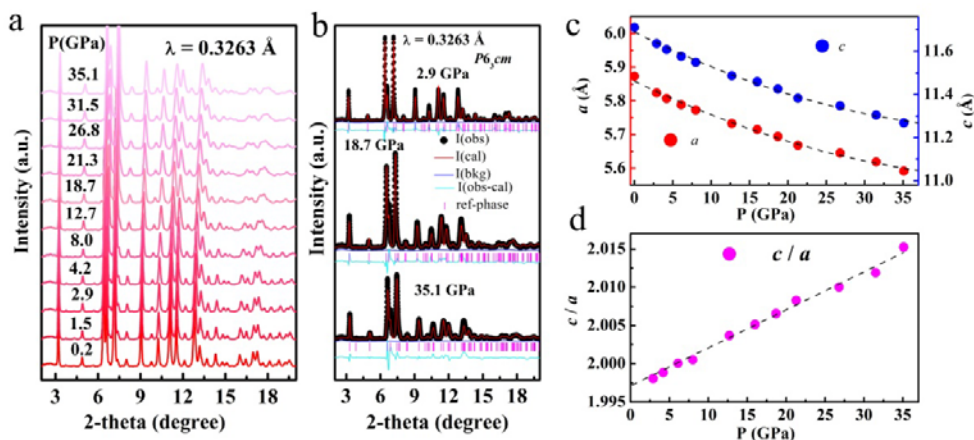


**FIG. 1. Structural information of pressurized hexagonal  $Lu_{0.5}Sc_{0.5}FeO_3$ , revealed from high pressure x-ray diffraction (XRD).** (a) X-ray diffraction patterns collected during the compressing process, with the incident X-ray wavelength of 0.3263  $\text{\AA}$  (b) GSAS refinement of XRD patterns at pressures 2.9 GPa, 18.7 GPa and 35.1 GPa. (c) Lattice constant  $a$  (red) and  $c$  (blue) evolutions under pressure, with the measured data in dots, and the dashed black lines are the fitted curves. The measured lattice constants ( $a=5.8735 \text{ \AA}$ ,  $c=11.7098 \text{ \AA}$ ) at ambient conditions are also shown here, with details in Section S1 of Supplementary Information. (d)  $c/a$  ratio versus pressure.

Rietveld refinement analysis further reveals that  $h$ -LSFO is non-uniformly compressed along the  $a$ - and  $c$ -axes directions. As shown in Fig. 1c, the lattice constant  $a$  decreases by 4.8% from 5.8735  $\text{\AA}$  to 5.5915  $\text{\AA}$  while the lattice constant  $c$  decreases by 3.8% from 11.7098  $\text{\AA}$  to 11.2683  $\text{\AA}$ , resulting in an increase of the  $c/a$  ratio to 2.015 (Fig. 1d). Note that this is the highest reported  $c/a$  ratio among the hexagonal rare earth ferrites [9,10]. The large pressure-induced  $c/a$  ratio may be attributed to several factors: 1) The Fe  $3d$  - O  $2p$  hybridization prefers to be along the  $c$ -axis, and therefore the out-of-plane lattice constant is much more stable against pressure [30]; 2) Structural distortion of  $FeO_5$  bipyramids may also play a significant role, as the tilting angle ( $\theta$ -angle demonstrated in Fig. 2a) increases under pressure, which is discussed in detail in Section S3 of [Supplemental Material \[27\]](#).

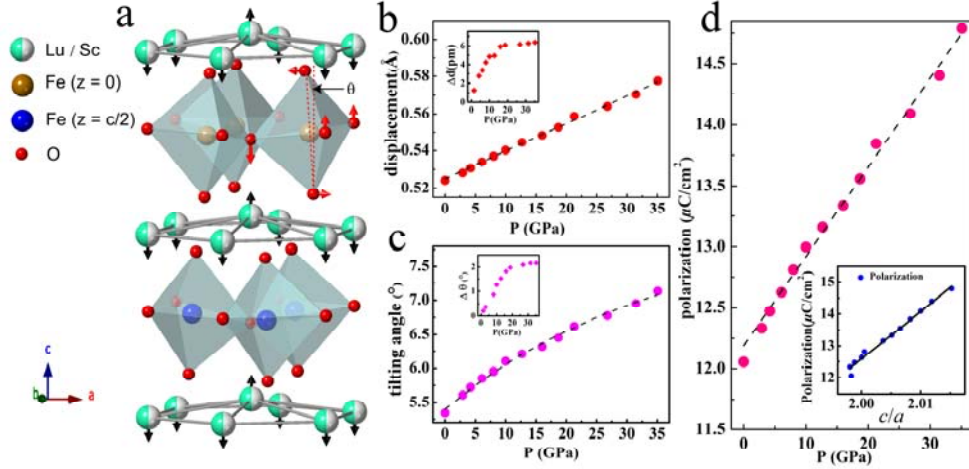


**FIG. 2. DFT calculation results of some properties in pressurized *h*-LSFO.** (a) 3D view of the crystal structure for the  $P6_3cm$  hexagonal space group. The red arrows are related to the tilting of  $\text{FeO}_5$  bipyramids associated with the “ $K_3$ ” mode, while the black arrows indicate the displacement of the Lu/Sc atoms within this “ $K_3$ ” mode. The tilting angle of  $\text{FeO}_5$  bipyramids is denoted as  $\theta$ . (b) High-pressure evolution of the displacement of Lu/Sc atoms in the Lu(Sc)-O layers and (c) tilting angle in the  $\text{FeO}_5$  bipyramids, with the lattice parameters obtained from XRD results, while the atomic positions are optimized until all Hellman-Feynman forces are smaller than  $0.01 \text{ eV}/\text{\AA}$  on each ion. Inset of b-c, experiment results of displacement (b) and tilting angle (c) extracted from GSAS refinement. The values along the x-axis represent the pressure, labeled as P (GPa). The values along the y-axis in the inset represent the experimental value of the relative (Value(High Pressure)-Value(ambient)) displacement (b, marked as  $\Delta d$ ) and tilting angle (c, marked as  $\Delta\theta$ .) The DFT results and the GSAS refinement results both show consistent trends of pressure induced enhancement of displacement and tilting angle. (d) Predicted electrical polarization *versus* pressure (inset, Polarization *versus*  $c/a$  ratio).

Previous studies demonstrated that hexagonal  $\text{Lu}_{0.5}\text{Sc}_{0.5}\text{FeO}_3$  exhibit an electric polarization that is induced by geometrical displacements [25,29], which originates from the buckling of Lu/Sc atoms (one up/two down) and the tilting of  $\text{FeO}_5$  bipyramids associated with the so-called “ $K_3$ ” mode. Such “ $K_3$ ” mode is a zone-boundary mode located at  $\frac{2\pi}{a}(\frac{1}{3}, \frac{1}{3}, 0)$ , where the atomic displacement of  $\text{FeO}_5$  include the two apical oxygen atoms with opposite directions in the  $ab$ -plane, and the three equatorial oxygen atoms with two up/one down along the  $c$ -direction [11,31], which is indicated by the red arrows in Fig. 2a. According to previous studies of  $\text{RFeO}_3$  and  $\text{RMnO}_3$  [12,32], It softens under pressure. Here, the GSAS (General Structure Analysis System software) refinement on the XRD patterns further shows that the Lu/Sc layers prefer to buckle under pressure, leading to a pressure-induced displacement enhancement (see inset of Fig. 2b). Moreover, the GSAS refinement also suggests that the  $\theta$  tilting



angle (Fig. 2a) of nearest-neighbor interlayer FeO layers increases under pressure (see inset of Fig. 2c). Therefore, the XRD data clearly indicate a pressure-induced enhancement of electric polarization in *h*-LSFO, as a result of this increase of the tilting angle and displacement.

DFT calculations are performed here to simulate the hydrostatic pressure effects on structural properties and electric polarization of *h*-LSFO. Figure 2a schematizes the relative displacements of Lu/Sc layers and the tilting of FeO<sub>5</sub> bipyramids, which constitute the so-called “*K*<sub>3</sub>” mode. As pressure is increased up to 35.1 GPa, the displacement of Lu/Sc layers increases by 11% (Fig. 2b), and the tilting angle of FeO<sub>5</sub> bipyramids is enhanced by 34% (Fig. 2c) in *h*-LSFO, as found from our DFT calculations. These results agree well with the GSAS refinement results of the XRD measurements (Inset of Fig. 2b-c, See Section S3 of [Supplementary Material](#) for details [27]). Such enhancement indicates that the strength of “*K*<sub>3</sub>” mode increases with increasing pressure, which is consistent with previous calculations on RFeO<sub>3</sub> and RMnO<sub>3</sub> [12,32]. The polarization, which is coupled with the “*K*<sub>3</sub>” mode, is determined to increase accordingly by 23%, from 12.0 μC/cm<sup>2</sup> at ambient pressure up to 14.8 μC/cm<sup>2</sup> at 35.1 GPa (Fig. 2d). Such pressure-induced polarization enhancement originates from the improper nature of the ferroelectricity in hexagonal YMnO<sub>3</sub>-type ferroelectrics. Therefore, in hexagonal ferrites and other improper ferroelectrics, the pressure can not only increase the *c/a* ratio, but also increases the displacement in R-layer atoms and the tilting angle of the FeO<sub>5</sub> trigonal bipyramid, which is the main reason for the dramatically enhanced polarization.

Besides the electric polarization, the evolution of  $T_N$  of *h*-LSFO under pressure is also calculated by DFT calculations and mean-field approximation. We adopt here the magnetic Hamiltonian  $H = \sum_{i,j} J \mathbf{S}_i \cdot \mathbf{S}_j$ , where the summation runs over all nearest-neighbor Fe-Fe pairs. The interlayer couplings are neglected, since previous studies show that they are much weaker than intralayer couplings [25]. The coupling coefficient,  $J$ , can be extracted from the total energies of ferromagnetic and antiferromagnetic configurations.  $T_N$  can then be estimated using the equation  $T_N = \frac{qJS^2}{3k_B}$ , where  $k_B$  is the Boltzmann constant,  $S = 5/2$  is the spin quantum number of Fe<sup>3+</sup> and  $q=6$  is the number of the nearest neighbors [33]. Note that  $J$  parameters under all pressures are rescaled by the same constant, which ensures the predicted  $T_N$  of the hexagonal LuFeO<sub>3</sub> to be consistent with the experimental value [5-8]. In addition, the spin structure used in the DFT calculation is shown in Fig. 3a and is consistent with the previous reported experiment results [10,34]. As shown in Fig. 3b, the predicted  $T_N$  of the

*h*-LSFO is 160 K at ambient pressure, which is quite close to our measured 167 K, testifying the accuracy of our calculations (once adopting the aforementioned rescaling). The calculated  $T_N$  increases monotonically with increasing pressure and reaches 228 K at 35.1 GPa, which is nearly 70 K higher than  $T_N$  at ambient condition. Moreover, Fig. 3b also shows that pressure has a much larger effect on  $T_N$  than chemical doping since the pressure-induced slope of  $T_N$  with increasing  $c/a$  ratio (the magenta dots and lines represent the calculated  $T_N$  of pressurized *h*-LSFO in Fig. 3b) is over 6 times larger than that induced by chemical doping (see Fig. 3b, where the blue dots represent the calculated  $T_N$  of *h*-RFeO<sub>3</sub> but for which the lattice parameters are extracted from measurements [4,35-36] while the red dots display experimental results [4-8]). The dramatic enhancement of  $T_N$  can be understood from the analysis of structural distortion and tilting angle of the FeO<sub>5</sub> bipyramids. As pressure increases to 35.1 GPa, the calculated tilting angle increases from 5.3° to 7.1° for *h*-LSFO (Fig. 2c), which is over six times larger than the increase of tilting angle induced by chemical doping (from 5.1° for TmFeO<sub>3</sub> to 5.3° for *h*-LSFO at ambient pressure, as shown in the inset of Fig.3c). As a summary of Fig. 3, it can be intuitively figured out that instead of increasing the  $c/a$  ratio, the remarkably enhanced tilting angle under pressure does matter for the dramatically  $T_N$  enhancement among the hexagonal ferrites.

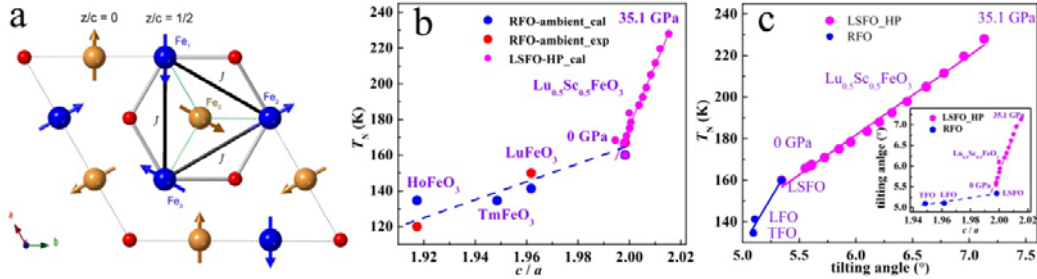


**FIG. 3. Density functional theory (DFT) calculation results of the magnetic transition temperature ( $T_N$ ) in *h*-RFeO<sub>3</sub> under chemical doping or hydrostatic pressure.** (a) The Nearest Neighbor (NN) super-exchange interactions between in-plane Fe atoms (J), the spin structure used for calculation is consistent with Refs [10,34]. (b)  $T_N$  versus the  $c/a$  ratio. Calculated  $T_N$  are shown via blue dots for hexagonal HoFeO<sub>3</sub> (HFO), TmFeO<sub>3</sub> (TFO), LuFeO<sub>3</sub> (LFO) and Lu<sub>0.5</sub>Sc<sub>0.5</sub>FeO<sub>3</sub> (LSFO) using the experimental lattice parameters for HFO [4], TFO [35], LFO [36] as inputs, while experimental results of  $T_N$  are shown via red dots for HFO [4], LFO [5-8] and LSFO (our experiment result). The calculated  $T_N$  of hexagonal Lu<sub>0.5</sub>Sc<sub>0.5</sub>FeO<sub>3</sub> under pressure is also displayed via magenta dots. (c) The calculated  $T_N$  versus tilting angle for *h*-RFeO<sub>3</sub> (blue dots) and *h*-Lu<sub>0.5</sub>Sc<sub>0.5</sub>FeO<sub>3</sub> (magenta dots), with the tilting angle versus  $c/a$  ratio being shown in the inset.

We now turn to discuss the correlation between the enhanced  $T_N$  of *h*-LSFO and the structural

distortion revealed by both DFT calculations and XRD measurements. As pressure increases, the distances between Fe atoms and the bond length between Fe and O atoms both decrease (See Fig. S2 [27]), leading to a stronger exchange interaction, and thus giving rise to an enhanced  $T_N$ . Besides, as pressure increases, the “ $K_3$ ” distortion is also enhanced, contributing to an enhancement of magnetic properties in  $h$ -LSFO (Fig. 3c), which is in-line with the theory analysis proposed by H. Das *et al.* in hexagonal  $\text{RMO}_3$  systems [11]. In addition, K. Sinha *et al.* also reported that  $T_N$  can be increased by enhancing structural distortion in hexagonal  $\text{ScFeO}_3$  films grown on  $\text{Al}_2\text{O}_3$  (001) substrate [37]. Moreover, the structural distortion can be much more dramatically enhanced at the case of applying hydrostatic pressure rather than the chemical doping (Fig. 3c) or strains arising from substrates, leading to a much more remarkable enhancement of  $T_N$ . In fact, the effectiveness of pressure to increase  $T_N$  reflects the fact that pressure has a more pronounced effect on structural distortion than previous methods (strain and chemical doping). As the crystal structure will go back to the ambient phase (See Fig. S3 [27]), and thus the  $T_N$  is also expected to go back to its value in the ambient phase. Therefore, further investigation of searching a quenchable high pressure hexagonal phase with enhanced structural distortion and reduced Fe-Fe distance is also deserved to be done among the hexagonal ferrites and systems alike.

In conclusion, we report that, and explain why, pressure can be an effective method to enhance multiferroicity of hexagonal ferrites. In particular, pressure can lead to a large increase of  $T_N$  as well as an enhancement of the polarization in hexagonal  $\text{Lu}_{0.5}\text{Sc}_{0.5}\text{FeO}_3$ . According to our calculation, similar behaviors are also expected in other hexagonal systems such as  $\text{RFeO}_3$  ( $\text{R} = \text{Y}, \text{Sc}, \text{rare earth Lu-Dy}$ ), and this behavior should also be valid for other hexagonal ferrites and other improper ferroelectrics.

### **Acknowledgements**

This work was supported by NSAF (Grant No. U1530402), National Key Research and Development Program of China (2016YFA0300702), National Basic Research Program of China (973 Program) under Grants No. 2014CB921104, National Natural Science Foundation of China (Grant No.11504053), the Program of Shanghai Academic Research Leader (No. 17XD1400400), and the Shanghai Municipal Natural Science Foundation (18JC1411400, 18ZR1403200). We acknowledge Dr. Changyong Park at 16BM-D, APS, ANL for the technical supports on the high-pressure XRD experiments. Portions of this work were performed at HPCAT (Sector 16), Advanced Photon Source (APS), Argonne National

Laboratory (ANL). HPCAT operations are supported by DOE-NNSA's Office of Experimental Sciences. The Advanced Photon Source is a U.S. Department of Energy (DOE) Office of Science User Facility operated for the DOE Office of Science by Argonne National Laboratory under Contract No. DE-AC02-06CH11357. Dr. Lili Zhang and Dr. Aiguo Li of 15U1 at SSRF (Shanghai Synchrotron Radiation Facility) were also acknowledged for the technical supports on the high-pressure XRD experiments at SSRF. C.X. and L.B. thank the financial support from the DOE, Office of Basic Energy Sciences, under Award # DE-SC0002220. H. X. acknowledges the support by NSFC, the Special Funds for Major State Basic Research (Grant No. 2015CB921700), the Qing Nian Ba Jian Program, and the Fok Ying Tung Education Foundation. S. S. and J. Z. were supported by the Ministry of Science and Technology of China (Program 973: 2015CB921302), the National Key R&D Program of the MOST of China (grant number 2016YFA0300203) and the Thousand-Youth-Talent Program of China.

## References

- [1] Y. Tokunaga, Y. Taguchi, T. Arima and Y. Tokura, *Nat. Phys.* **8**, 838 (2012).
- [2] S. Artyukhin, K. T. Delaney, N. A. Spaldin, and M. Mostovoy, *Nat. Mater.* **13**, 42 (2014).
- [3] M. Ye and D. Vanderbilt, *Phys. Rev. B* **92**, 035107 (2015).
- [4] A. R. Akbashev, A. S. Semisalova, N. S. Perov, and A. R. Kaul, *Appl. Phys. Lett.* **99**, 122502 (2011).
- [5] W. Wang, J. Zhao, W. Wang, Z. Gai, N. Balke, M. Chi, H. Lee, W. Tian, L. Zhu, X. Cheng, D. J. Keavney, J. Yi, T. Z. Ward, P. C. Snijders, H. M. Christen, W. Wu, J. Shen, and X. Xu, *Phys. Rev. Lett.* **110**, 237601 (2013).
- [6] J. A. Moyer, R. Misra, J. A. Mundy, C. M. Brooks, J. T. Heron, D. A. Muller, D. G. Schlom, and P. Schiffer, *APL Mater.* **2**, 012106 (2014).
- [7] P. Suresh, K. V. Laxmi, A. K. Bera, S. M. Yusuf, B. L. Chittari, J. Jung, and P. S. Anil Kumar, *Phys. Rev. B* **97**, 184419 (2018).
- [8] S. M. Disseler, J. A. Borchers, C. M. Brooks, J. A. Mundy, J. A. Moyer, D. A. Hillsberry, E. L. Thies, D. A. Tenne, J. Heron, M. E. Holtz, J. D. Clarkson, G. M. Stiehl, P. Schiffer, D. A. Muller, D. G. Schlom, and W. D. Ratcliff, *Phys. Rev. Lett.* **114**, 217602 (2015).
- [9] X. Xu, and W. Wang, *Mod. Phys. Lett. B* **28**, 1430008 (2014).
- [10] S. M. Disseler, X. Luo, B. Gao, Y. S. Oh, R. Hu, Y. Wang, D. Quintana, A. Zhang, Q. Huang, J. Lau, R. Paul, J. W. Lynn, S.-W. Cheong, and W. Ratcliff, II, *Phys. Rev. B* **92**, 054435 (2015).

- [11] Hena Das, Aleksander L. Wysocki, Yanan Geng, Weida Wu & Craig J. Fennie, *Nat. Commun.* **5**, 2998 (2014).
- [12] C. Xu, Y. Yang, S. Wang, W. Duan, B. Gu, and L. Bellaiche, *Phys. Rev. B* **89**, 205122 (2014).
- [13] Note that the fully optimized  $c/a$  ratio from simulations follows the same trend with our experimental one that the  $c/a$  ratio increases when increasing pressure
- [14] J. R. Carvajal, *Physica B: Condens. Matter* **192**, 55 (1993).
- [15] X. F. Chen, X. L. Dong, F. Cao, J. X. Wang, and G. S. Wang, *J. Am. Ceram. Soc.* **97**, 213 (2014).
- [16] H. K. Mao, P. M. Bell, K. J. Dunn, R. M. Chrenko, and R. C. DeVries, *Rev. Sci. Instrum.* **50**, 1002 (1979).
- [17] S. Klotz, J.-C. Chervin, P. Munsch, and G. L. Marchand, *J. Appl. Phys. D: Appl. Phys.* **42**, 075413 (2009).
- [18] H. K. Mao, J. Xu, and P. M. Bell, *J. Geophys. Res., Solid Earth* **91**, 4673 (1986).
- [19] C. Prescher, and V. B. Prakapenka, *High Pressure Research*. **35**, 223 (2015).
- [20] H. M. Rietveld, *J. Appl. Cryst.* **2**, 65 (1969).
- [21] B. H. Toby, and R. B. Von Dreele, *J. Appl. Cryst.* **46**, 544 (2013).
- [22] G. Kresse, and D. Joubert, *Phys. Rev. B* **59**, 1758 (1999).
- [23] J. P. Perdew, A. Ruzsinszky, G. I. Csonka, O. A. Vydrov, G. E. Scuseria, L. A. Constantin, X. Zhou, and K. Burke, *Phys. Rev. Lett.* **100**, 136406 (2008),
- [24] P. E. Blöchl, *Phys. Rev. B* **50**, 17953 (1994).
- [25] L. Lin, H. M. Zhang, M. F. Liu, S. Shen, S. Zhou, D. Li, X. Wang, Z. B. Yan, Z. D. Zhang, J. Zhao, S. Dong, and J.-M. Liu, *Phys. Rev. B* **93**, 075146 (2016).
- [26] R. D. King-Smith and D. Vanderbilt, *Phys. Rev. B* **47**, 1651(R) (1993).
- [27] See Supplemental Material at [URL] for the details of sample characterization at ambient pressure, detailed discussion of phase stability of  $o$ -phase and  $h$ -phase of  $R\text{FeO}_3$ , details of displacement, tilting angle and bond length evolution results extracted from GSAS refinement, and the detailed discussion of XRD patterns collected during decompress process.
- [28] A. Masuno, A. Ishimoto, C. Moriyoshi, H. Kawaji, Y. Kuroiwa, and H. Inoue, *Inorg. Chem.* **54**, 9432 (2015).
- [29] K. Du, B. Gao, Y. Wang, X. Xu, J. Kim, R. Hu, F.-T. Huang and S.-W. Cheong, *npj Quantum Materials* **3**, 33 (2018).

- [30] S. Cao, X. Zhang, T. R Paudel, K. Sinha, X. Wang, X. Jiang, W. Wang, S. Brutsche, J. Wang, P. J Ryan, J.-W. Kim, X. Cheng, E. Y Tsymbal, P. A Dowben and X. Xu, *J. Phys.: Condens. Matter* **28**, 156001 (2016).
- [31] H. Wang, I. V. Solovyev, W. Wang, X. Wang, P. J. Ryan, D. J. Keavney, J.-W. Kim, T. Z. Ward, L. Zhu, J. Shen, X. M. Cheng, L. He, X. Xu, and X. Wu, *Phys. Rev. B* **90**, 014436 (2014).
- [32] H. Tan, C. Xu, M. Li, S. Wang, B.-L. Gu and W. Duan, *J. Phys.: Condens. Matter* **28**, 126002 (2016).
- [33] S. V. Halilov, H. Eschrig, A. Y. Perlov, and P. M. Oppeneer, *Phys. Rev. B* **58**, 293 (1998).
- [34] J. C. Leiner, Taehun Kim, Kisoo Park, Joosung Oh, T. G. Perring, H. C. Walker, X. Xu, Y. Wang, S.-W. Cheong, and Je-Geun Park, *Phys. Rev. B* **98**, [134412](#) (2018).
- [35] A. A. Bossak, I. E. Graboy, O. Y. Gorbenko, A. R. Kaul, M. S. Kartavtseva, V. L. Svetchnikov, and H. W. Zandbergen, *Chem. Mater.* **16**, [1751](#) (2004).
- [36] E. Magome, C. Moriyoshi, Y. Kuroiwa, A. Masuno, and H. Inoue, *Jpn. J. Appl. Phys.* **49**, 09ME06 (2010).
- [37] K. Sinha, H. Wang, X. Wang, L. Zhou, Y. Yin, W. Wang, X. Cheng, D. J. Keavney, H. Cao, Y. Liu, X. Wu, and X. Xu. *Phys. Rev. Lett.* **121**, 237203 (2018).